

# Bimodal-sized quantum dots for broad spectral bandwidth emitter

Yinli Zhou, Jian Zhang,\* Yongqiang Ning, Yugang Zeng, Jianwei Zhang, Xing Zhang, Li Qin, and Lijun Wang

State Key Laboratory of Luminescence and Applications, Changchun Institute of Optics, Fine Mechanics and Physics, Chinese Academy of Sciences, Changchun, China

\*jzhang@ciomp.ac.cn

**Abstract:** In this work, a high-power and broadband superluminescent diode (SLD) is achieved utilizing bimodal-sized quantum dots (QDs) as active materials. The device exhibits a 3 dB bandwidth of 178.8 nm with output power of 1.3 mW under continuous-wave (CW) conditions. Preliminary discussion attributes the spectra behavior of the device to carrier transfer between small dot ensemble and large dot ensemble. Our result provides a new possibility to further broadening the spectral bandwidth and improving the CW output power of QD-SLDs.

©2015 Optical Society of America

**OCIS codes:** (250.0250) Optoelectronics; (230.5590) Quantum-well, -wire and -dot devices; (230.3670) Light-emitting diodes.

---

## References and links

1. W. K. Burns, C. Chen, and R. P. Moeller, "Fiber-optic gyroscopes with broad-band sources with broad-band sources," *J. Lightwave Technol.* **1**(1), 98–105 (1983).
2. S.-J. Park, C.-H. Lee, K.-T. Jeong, H.-J. Park, J.-G. Ahn, and K.-H. Song, "Fiber-to-the-Home Services Based on Wavelength-Division-Multiplexing Passive Optical Network," *J. Lightwave Technol.* **22**(11), 2582–2591 (2004).
3. K. H. Yoon, S. H. Oh, K. S. Kim, O. K. Kwon, D. K. Oh, Y. O. Noh, and H. J. Lee, "2.5-Gb/s hybridly-integrated tunable external cavity laser using a superluminescent diode and a polymer Bragg reflector," *Opt. Express* **18**(6), 5556–5561 (2010).
4. M. D. Bayleyegn, H. Makhoulf, C. Crotti, K. Plamann, and A. Dubois, "Ultrahigh resolution spectral-domain optical coherence tomography at 1.3 $\mu$ m using a broadband superluminescent diode light source," *Opt. Commun.* **285**(24), 5564–5569 (2012).
5. A. F. Fercher, W. Drexler, C. K. Hitzenberger, and T. Lasser, "Optical coherence tomography—principles and applications," *Rep. Prog. Phys.* **66**(2), 239–303 (2003).
6. Y. Wang, J. Nelson, Z. Chen, B. Reiser, R. Chuck, and R. Windeler, "Optimal wavelength for ultrahigh-resolution optical coherence tomography," *Opt. Express* **11**(12), 1411–1417 (2003).
7. M. C. Pierce, J. Strasswimmer, B. H. Park, B. Cense, and J. F. de Boer, "Advances in optical coherence tomography imaging for dermatology," *J. Invest. Dermatol.* **123**(3), 458–463 (2004).
8. S. Chen, K. Zhou, Z. Zhang, J. R. Orchard, D. T. D. Childs, M. Hugues, O. Wada, and R. A. Hogg, "Hybrid quantum well quantum dot structure for broad spectral bandwidth emitters," *IEEE J. Sel. Top. Quantum* **19**(4), 1900209 (2013).
9. M. Z. M. Khan, H. H. Alhashim, T. K. Ng, and B. S. Ooi, "High-power and high-efficiency 1.3 $\mu$ m superluminescent diode with flat-top and ultrawide emission bandwidth," *IEEE Photonics J.* **7**(1), 1–8 (2015).
10. H. Wang, H. Yu, X. Zhou, Q. Kan, L. Yuan, W. Chen, W. Wang, Y. Ding, and J. Pan, "High-power InGaAs/GaAs quantum-well laser with enhanced broad spectrum of stimulated emission," *Appl. Phys. Lett.* **105**(14), 141101 (2014).
11. Z. Z. Sun, D. Ding, Q. Gong, W. Zhou, B. Xu, and Z. G. Wang, "Quantum-dot superluminescent diode A proposal for an ultra-wide output spectrum," *Opt. Quantum Electron.* **31**(12), 1235–1246 (1999).
12. L. H. Li, M. Rossetti, A. Fiore, L. Occhi, and C. Velez, "Wide emission spectrum from superluminescent diodes with chirped quantum dot multilayers," *Electron. Lett.* **41**(1), 41–43 (2005).
13. S. Haffouz, P. J. Barrios, R. Normandin, D. Poitras, and Z. Lu, "Ultrawide-bandwidth, superluminescent light-emitting diodes using InAs quantum dots of tuned height," *Opt. Lett.* **37**(6), 1103–1105 (2012).
14. X. Li, P. Jin, Q. An, Z. Wang, X. Lv, H. Wei, J. Wu, J. Wu, and Z. Wang, "Experimental investigation of wavelength-selective optical feedback for a high-power quantum dot superluminescent device with two-section structure," *Opt. Express* **20**(11), 11936–11943 (2012).
15. M. Z. Khan, M. A. Majid, T. K. Ng, D. Cha, and B. S. Ooi, "Simultaneous quantum dash-well emission in a chirped dash-in-well superluminescent diode with spectral bandwidth >700 nm," *Opt. Lett.* **38**(19), 3720–3723 (2013).

16. J. Johansson, W. Seifert, T. Junno, and L. Samuelson, "Sizes of self-assembled quantum dots—effects of deposition conditions and annealing," *J. Cryst. Growth* **195**(1–4), 546–551 (1998).
17. J. Johansson and W. Seifert, "Kinetics of self-assembled island formation: Part II—Island size," *J. Cryst. Growth* **234**(1), 139–144 (2002).
18. H. Lee, R. Lowe-Webb, T. J. Johnson, W. Yang, and P. C. Sercel, "Photoluminescence study of in situ annealed InAs quantum dots: Double-peak emission associated with bimodal size distribution," *Appl. Phys. Lett.* **73**(24), 3556–3558 (1998).
19. G. Saint-Girons, G. Patriarche, A. Mereuta, and I. Sagnes, "Origin of the bimodal distribution of low-pressure metal-organic-vapor-phase-epitaxy grown InGaAs/GaAs quantum dots," *J. Appl. Phys.* **91**(6), 3859–3863 (2002).
20. S. J. Lee, S. K. Noh, J. W. Choe, and E. K. Kim, "Evolution of bimodal size-distribution on InAs coverage variation in as-grown InAs/GaAs quantum-dot heterostructures," *J. Cryst. Growth* **267**(3–4), 405–411 (2004).
21. B. Bhavtosh, "A model for the temperature dependence of photoluminescence from self-assembled quantum dots," *J. Appl. Phys.* **100**(9), 093107 (2006).
22. G. Saint-Girons, G. Patriarche, L. Largeau, J. Coelho, A. Mereuta, J. M. Moison, J. M. Gérard, and I. Sagnes, "Bimodal distribution of Indium composition in arrays of low-pressure metalorganic-vapor-phase-epitaxy grown InGaAs/GaAs quantum dots," *Appl. Phys. Lett.* **79**(14), 2157–2159 (2001).
23. T. B. Norris, K. Kim, J. Urayama, Z. K. Wu, J. Singh, and P. K. Bhattacharya, "Density and temperature dependence of carrier dynamics in self-organized InGaAs quantum dots," *J. Phys. D Appl. Phys.* **38**(13), 2077–2087 (2005).
24. G. Saint-Girons and I. Sagnes, "Photoluminescence quenching of a low-pressure metal-organic vapor-phase-epitaxy grown quantum dots array with bimodal inhomogeneous broadening," *J. Appl. Phys.* **91**(12), 10115 (2002).
25. W. M. Schulz, R. Roßbach, M. Reischle, G. J. Beirne, M. Bommer, M. Jetter, and P. Michler, "Optical and structural properties of InP quantum dots embedded in  $(\text{Al}_x\text{Ga}_{1-x})_{0.51}\text{In}_{0.49}\text{P}$ ," *Phys. Rev. B* **79**(3), 035329 (2009).
26. G. Muñoz-Matutano, I. Suárez, J. Canet-Ferrer, B. Alén, D. Rivas, L. Seravalli, G. Trevisi, P. Frigeri, and J. Martínez-Pastor, "Size dependent carrier thermal escape and transfer in bimodally distributed self assembled InAs/GaAs quantum dots," *J. Appl. Phys.* **111**(12), 123522 (2012).
27. H. Kissel, U. Müller, C. Walther, W. T. Masselink, Y. I. Mazur, G. G. Tarasov, and M. P. Lisitsa, "Size distribution in self-assembled InAs quantum dots on GaAs (001) for intermediate InAs coverage," *Phys. Rev. B* **62**(11), 7213–7218 (2000).
28. S. Grosse, J. H. H. Sandmann, G. von Plessen, J. Feldmann, H. Lipsanen, M. Sopanen, J. Tulkki, and J. Ahopelto, "Carrier relaxation dynamics in quantum dots: Scattering mechanisms and state-filling effects," *Phys. Rev. B* **55**(7), 4473–4476 (1997).
29. C. Y. Ngo, S. F. Yoon, W. J. Fan, and S. J. Chua, "Effects of size and shape on electronic states of quantum dots," *Phys. Rev. B* **74**(24), 245331 (2006).
30. S. I. Jung, H. Y. Yeo, I. Yun, J. Y. Leem, I. K. Han, J. S. Kim, and J. I. Lee, "Photoluminescence study on the growth of self-assembled InAs quantum dots: formation characteristics of bimodal-sized quantum dots," *Physica E* **33**(1), 280–283 (2006).

## 1. Introduction

Superluminescent diodes (SLDs) are ideal broadband optical sources for many applications, such as fiber-optic gyroscopes [1], wavelength-division-multiplexing systems [2], tunable external cavity laser [3], and optical coherence tomography (OCT) [4] because of their advantages like compact size, high efficiency, and cost-effectiveness. Recently, more and more interest has been focused upon applications in OCT system, where the wavelength range of 1000–1300 nm is important for imaging in the biological "window". For instance, the center wavelength of 1050 nm [5, 6] is typically used for ophthalmology and 1200–1300 nm [7] for skin imaging due to the minimum of optical dispersion in water, and the minimum in scattering and absorption, respectively [8]. High power and wide bandwidth are two main parameters of SLDs which are simultaneously required for achieving higher axial resolution, improved signal-to-noise ratio, and penetration depth in an OCT system. To achieve these purposes, various semiconductor structures have been proposed, including multiple quantum wells [9] and tunnel injection quantum wells [10]. Recently, SLDs with QD based active materials have attracted increasing interest due to the large inhomogeneous distribution of the self-assembled QDs and simultaneous two-state lasing from the ground state (GS) and excited state (ES) from QDs [11]. Combining these two natural characteristics, an ultrawide emission spectrum may be achieved. To date, considerable efforts have been made in developing high-power and broadband QD-SLD devices including chirped QDs, hybrid QW/QD structure and multi-section device and so on. By using chirped QDs technique, a SLD incorporating InAs QDs capped with different InGaAs strain reducing layer(SRL) has

been reported with a bandwidth of 121 nm and output power of 1.3 mW under pulsed operation [12]. Through carefully tuning the height of InAs QDs, a 190 nm broadband QD-SLD has been realized with CW output power of 0.54 mW [13]. An emission spectrum of 65 nm QD-SLD with output power of 338 mW has been achieved by using two-section structure [14]. More recently, ultra-broad spectral bandwidth > 700 nm has been realized through simultaneous quantum dash-well emission in a hybrid QW/QD structure with chirped dash-in-well design [15].

Although QD-SLDs have achieved ultra broadband emission with hundreds of nanometers, the output power is still rather low especially under continuous injection. The main idea of the literatures above is to dislocate the emission peaks of separated active layers by varying the structure or tuning the size from one layer to another, which maybe named “varying design”. The “varying design” structure can simply broaden the emission bandwidth, but each layer only contribute to a relatively narrow emission bandwidth, which resulting in low gain and further causing low output power.

In this letter, we demonstrated a novel method of utilizing intentional bimodal-sized InGaAs/GaAs QDs to balance the spectral bandwidth and power. In distinction from the reported chirped QDs and hybrid QW/QD structures which use the “varying design” for separated layers in the active region, we introduce the bimodal-sized QDs which consist of quantum dots with two distinct sizes in one layer. The device containing five layers repeated bimodal-size QDs exhibits a 3 dB bandwidth of 178.8 nm and output power of 1.3 mW under CW conditions. One can think that we only used one single layer of quantum dot to achieve a 178.8 nm broadband output. This result, to our knowledge, is the best value in terms of emission from single layer of quantum dot. Our results provide a new possibility which can be combined with the above-mentioned “varying design” to further broadening the spectral bandwidth and improving the CW output power of QD-SLDs.

## 2. Experiment

The epitaxial structure of the bimodal-sized QD-SLD devices was grown by an AIXTRON 200-4 MOCVD system on an n-GaAs (001) substrate. The active region consists of repeated five  $\text{In}_{0.5}\text{Ga}_{0.5}\text{As}$  QD layers embed in six 40nm-GaAs space layers. The bimodal-sized QDs were all deposited at 530 °C with the same amount of 5.26 monolayers (MLs) and ultra-high growth rate of 1.64 ML/s. It has been demonstrated that these growth conditions help to form bimodal-sized quantum dot distribution [16, 17]. The initial 10 nm of the GaAs space layer was deposited at the same temperature of the QD layer to prevent the decomposition of quantum dots, and then the temperature was increased to 650 °C for the remaining 30 nm to reduce dot defect in the active region. An asymmetric graded index-separating confinement heterostructure (GRINSCH) was used for carrier confinement. The waveguide layer consists of  $\sim 3.7\ \mu\text{m}$  and  $\sim 1.7\ \mu\text{m}$  thick n- and p-type AlGaAs cladding layer with Si and Zn dopant, respectively. The detailed structure of the device is shown in Fig. 1.

Laser diodes with 8  $\mu\text{m}$  ridge width and broad-area SLDs with 90  $\mu\text{m}$  ridge width were fabricated by conventional lithography and wet chemical etching before a 300 nm  $\text{SiO}_2$  insulating layer was grown by Plasma-Enhanced Chemical Vapor Deposition (PECVD). Ti/Pt/Au and Ni/Ge/Au/Ni/Au ohmic contacts were evaporated on the top and back of the wafer, respectively. After anti-reflection coating on both facets of the SLDs, the wafers were cleaved into  $1.5\ \text{mm} \times 500\ \mu\text{m}$  individual chips and then mounted p-side up on a copper sink using an indium solder.

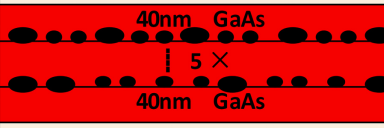
100nm	GaAs	Zn: $2 \times 10^{19}$
500nm	$\text{Al}_{0.20}\text{GaAs}$	Zn: $2 \times 10^{18}$
600nm	$\text{Al}_{0.10-0.12}\text{GaAs}$	Zn: $4 \times 10^{17}-1 \times 10^{18}$
450nm	$\text{Al}_{0.085-0.10}\text{GaAs}$	Zn: $1 \times 10^{17}-4 \times 10^{17}$
150nm	$\text{Al}_{0.08-0.085}\text{GaAs}$	Undoped
		
165nm	$\text{Al}_{0.08-0.05}\text{GaAs}$	Undoped
750nm	$\text{Al}_{0.09-0.08}\text{GaAs}$	Si: $2 \times 10^{17}-1 \times 10^{17}$
750nm	$\text{Al}_{0.10-0.09}\text{GaAs}$	Si: $4 \times 10^{17}-2 \times 10^{17}$
750nm	$\text{Al}_{0.11-0.10}\text{GaAs}$	Si: $1 \times 10^{18}-4 \times 10^{17}$
750nm	$\text{Al}_{0.12-0.11}\text{GaAs}$	Si: $2 \times 10^{18}-1 \times 10^{18}$
550nm	$\text{Al}_{0.15}\text{GaAs}$	Si: $2 \times 10^{18}$
20nm	$\text{Al}_{0.03-0.15}\text{GaAs}$	Si: $2 \times 10^{18}$
300nm	GaAs buffer	Si: $2 \times 10^{18}$
GaAs substrate		

Fig. 1. The epitaxial structure of the SLD.

### 3. Result and discussion

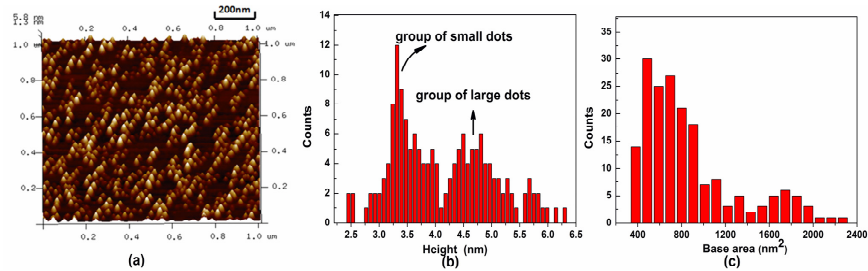


Fig. 2. (a) AFM image of uncapped samples. Size distribution of (b) height and (c) base area of QD sample.

AFM image and size distribution of the uncapped QD sample is presented in Fig. 2. Two groups of QDs with different size can be distinguished obviously. The “small dots (SDs)” have an average size of 3.5 nm in height, whereas the “large dots (LDs)” are 4.8 nm in height. Bimodal size distribution of quantum dots is a general feature of most materials systems undergoing self-assembled island growth based on the Stranski–Krastanow (S-K) growth mode and has been reported by many groups [18–21]. It has been demonstrated that this feature is beneficial to broaden the emission spectral of QDs [22]. According to the theoretical calculation of the electron state energy as a function of the pyramidal QD volume [29], the energy spacing between ground state of small dots (SD GS) and excited state of large dots (LD ES) can be very small. The wavelength space between LD ES and SD GS could be very small which is found in the following photoluminescence (PL) and electroluminescence (EL) spectrum of our devices.

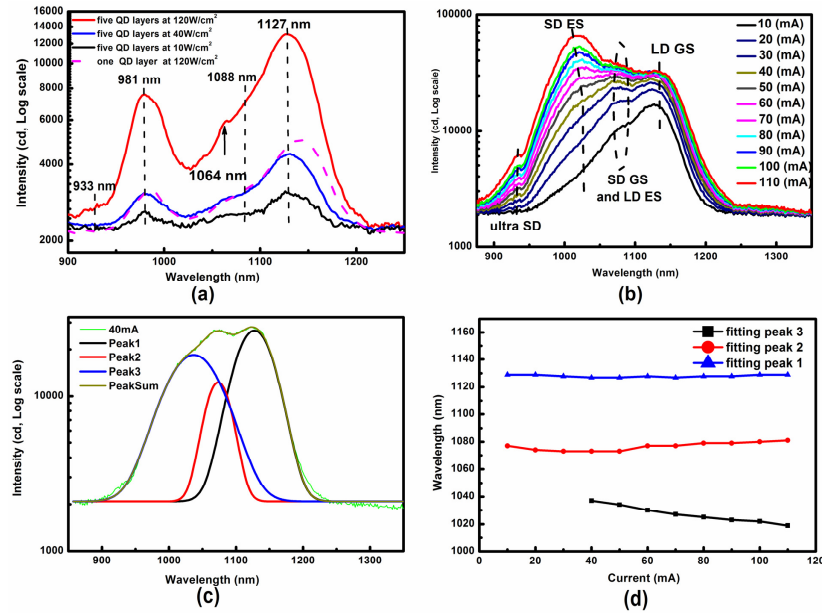


Fig. 3. (a) Intensity dependent PL of the full SLD structure which contains five QD layers and the sample contains one QD layer. (b) EL spectrum measured from the fabricated 8  $\mu\text{m}$  ridge width QD SLD at different inject current under pulsed condition. (c) Illustrating of Gaussian fitting of the EL curve at current of 40 mA. (d) Variation of the fitting peak position obtained from the fitting of the EL curve at different current.

Figure 3(a) depicts the intensity dependent photoluminescence measurement from the full SLD structure which contains five QD layers and the sample contains one QD layer. There is a peak around 1091 nm with broad FWHM of 82 nm according to the fitting result (not shown here) of the PL at excitation power density of 120 W/cm<sup>2</sup>. We consider that there must be different contributions to this peak. We fitted the EL spectrum at different current with three fitting peaks around 1018 nm, 1080 nm and 1125 nm. The variation of fitting peaks is shown in Fig. 3(d). Only two peaks were found around 1125 nm and 1080 nm when the current is less than 40 mA. The fitting peak 1 keeps almost unchanged as current increases. We attribute it to the emission from ground state of large dots (LD GS). The fitting peak 3 blueshift with increasing current. We attribute it to the emission from excited state of small dots (SD ES), and the blueshift is due to energy band reconstruction. The fitting peak 2 blueshift slightly first and then redshift as the current increases. It is inconsistent with the variation feature of the emission from LD ES which should blueshift like variation of fitting peak 3 due to energy band reconstruction. We believe that the emission around 1080 nm is composed of two contributions, one from the LD ES and the other from the SD GS, which is similar with the situation in [30]. The interfering signal at 1064 nm originates from excitation source. The peak appears at 981 nm in PL spectrum dose not appears in the EL spectrum at any injection current. We attribute it to the emission from the wetting layer of our samples, because under optical excitation condition, the photogenic charge carriers in wetting layer can participate in recombination luminescence in situ. By contrast, under electric injection, carriers will preferentially transfer to the lowest energy level lies in QDs and recombine there. Wetting layer only plays as a medium for carrier transportation under electric injection condition.

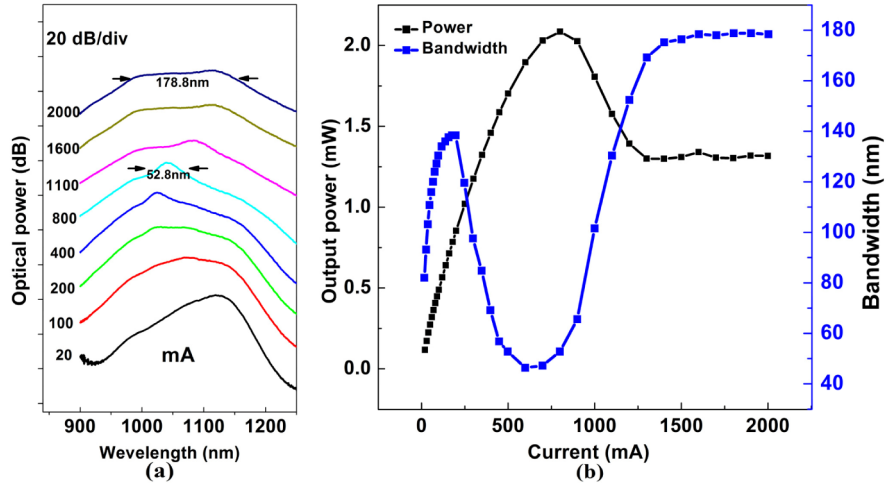


Fig. 4. (a) Room temperature CW emission spectrum at different injection current (b) Changes in power and bandwidth with injection current of the fabricated  $90\mu\text{m}$  ridge width QD-SLD device.

Figure 4(a) shows the output power spectrum of the fabricated SLD device as a function of the injection current under CW. An ultra-broad and flop-top emission profile is obtained with 3 dB bandwidth of 178.8 nm and 10 dB bandwidth of 308.2 nm at injection current of 2000 mA. The summary of SLD characteristics as a function of injection current, at room temperature, is shown in Fig. 4(b). At low injection current condition ( $I < 200$  mA), the power and bandwidth are both growing with the increase of current. Increasing the injection current from 200 mA to 800 mA has resulted in the power rising while the bandwidth narrowing rapidly. At a current of 800 mA, a broadband emission centered on 1040 nm with a bandwidth of 52.8 nm and maximum output power of 2.09 mW was obtained. Further increasing injection current to 1500 mA induces decreasing of the output power, but the bandwidth broadening rapidly at the same time. Above an injection current of 1500 mA, the output kept stable with power of 1.3 mW and 3 dB bandwidth of 178.8 nm. Based on the above, we consider that bimodal-sized QDs is an effective scheme for high power broadband SLD operating under CW condition.

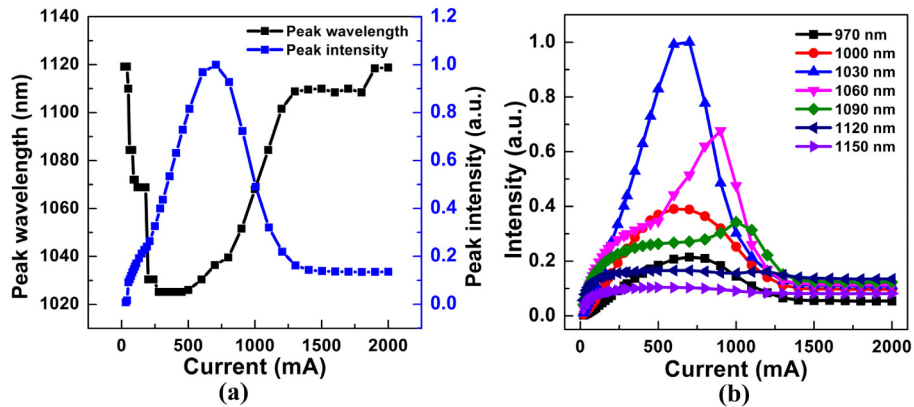


Fig. 5. (a) Variation of peak wavelength and peak intensity. (b) Intensity variation of some particular wavelength with the injection current of the QD-SLD under CW condition at room temperature.

Figure 5(a) shows the variation feature of peak wavelength as a function of the injection current. The intensity of the peak increased at first and decreased subsequently with increasing the injection current, while the peak wavelength blueshift at first and then redshift. In order to explain the complicated changes, we further investigated the intensity variation of some particular wavelength with the injection current. As shown obviously in Fig. 5(b), only a few short wavelengths ( $< 1090$  nm) have the similar intensity changes with the peak wavelength shown in Fig. 5(a). For the longer wavelength, especially 1150 nm, the intensity almost keep unchanged after a brief rise at the beginning.

There have been many studies on the carrier dynamics of bimodal-sized quantum dots. Various theoretical understanding have been proposed like: i) thermally excited carriers can reach non-radiative recombination centers at the heterostructure interface or in the barrier [23]; ii) thermally activated carriers transfer from high-energy QD ensembles to low-energy ensembles [24]; iii) the carrier redistribution favors the large dot due to the small energy-level spacing and low energy-level [25]; iiiii) the escape of exciton recede as the dot size becomes large [26]. Although these theories are based on the experimental results of temperature-dependent photoluminescence behavior of bimodal-sized quantum dots, different from the continuous electric injection situation at room temperature, we can still get some helpful enlightenment among them. Figure 6(a) depicts the situation when LD ensemble dominates the spectrum at low injection current ( $I < 200$  mA). This can be attributed to the low energy-level and small energy-level spacing of LD ensemble. When the injection current increase from 200 mA to 800 mA, as shown in Fig. 6(b), all the energy levels of the LD ensemble have been saturated, and carriers begin to fill higher energy-level in the SD ensemble. A disproportionate increase in gain for short wavelengths relate to SD ensemble result in spectral narrowing. Further increasing injection current to 1500 mA induces the junction temperature drastically rise and carriers escaping out of the QD. We consider that the thermal escape of carriers take place more easily in SD ensemble than in LD ensemble [27], while the thermally escaped carriers will be retrapped by LD ensemble to compensate the escaped carriers [28]. These processes lead to the quenching of high energy band and stable emission of low energy band. However, deeper consideration is still needed to explain clearly why there is a stable radiative recombination across a large spectral region (about 180 nm) at high injection current.

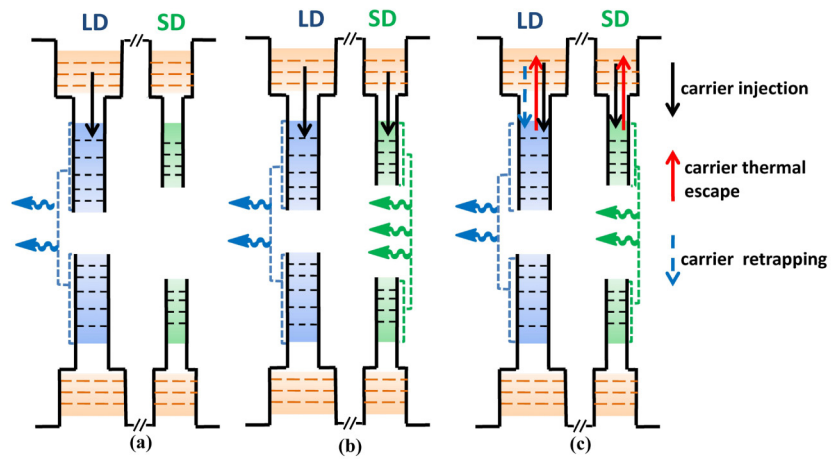


Fig. 6. Energy band model sketch of the bimodal-sized QD SLD showing the dominant emissions from large dot (LD) and small dot (SD) ensemble at (a) low, (b) moderate, and (c) high injection current. Blue and olive colors correspond to the available states of the LD group and SD group, while black, red, and blue arrows correspond to the carrier injection, carrier thermal escape, and carrier retrapping, respectively.

#### **4. Conclusion**

In summary, we demonstrated a new QD SLD which contains two different size of quantum dot. A stable emission spectrum with 3 dB bandwidth of 178.8 nm and output power of 1.3 mW at room temperature under CW condition is realized. Preliminary discussion attributes the spectra behavior of the device to carrier transfer between small dot ensemble and large dot ensemble. Finally, our result provides a new possibility to further broadening the spectral bandwidth and improving the CW output power of QD-SLDs.

#### **Acknowledgments**

This work was supported by the the National Natural Science Foundation of China (NSFC) (Nos. 61434005, 61376070, and 61234004).